Designing Heterocyclic Covalent Organic Frameworks with Tunable Electronic Structures for Efficient Electrosynthesis of Hydrogen Peroxide

Zhongjie Yang*[1], Lulu Zuo,[3] Bifu Luo,[1] Caoyu Yang,[3] Shi-Qiang Wang [2], Litian Chew,[2] Jun Zhu,[2]* Xiaofei Zhang[2]*

[1]School of Chemistry and Materials, Guizhou Normal University, Guiyang 550001, China
[2]Institute of Materials Research and Engineering (IMRE), Agency for Science, Technology and Research (A*STAR), Singapore 138634, Singapore
[3]CAS Key Laboratory of Nanosystem and Hierarchical Fabrication, CAS Center for Excellence in Nanoscience, National Center for Nanoscience and Technology, Chinese Academy of Sciences, Beijing 100190, China
* Corresponding authors.
Emails: zjyanggznu2022@foxmail.com (Zhongjie Yang), zhuj@imre.a-star.edu.sg (Jun Zhu), xiaofei@imre.a-star.edu.sg (Xiaofei Zhang)

Keywords: covalent organic frameworks, tunable electronic structures, oxygen reduction reaction, hydrogen peroxide electrosynthesis

Abstract:
The electrocatalytic production of hydrogen peroxide (H_2O_2) through the two-electron oxygen reduction reaction ($2e^-$ ORR) has garnered significant research attention in recent years due to its numerous appealing advantages, such as being eco-friendly and exhibiting high energy conversion efficiency. Metal-free carbon materials with specific catalytic sites have been recognized as potential electrocatalysts for $2e^-$ ORR; however, the design of highly efficient catalysts with well-defined structures and long-term stabilities for practical H_2O_2 production remains unsatisfactory. In this study, three covalent organic frameworks (COFs) – imine-linked LZU-1, oxazole-linked LZU-190, and thiazole-linked LZU-190(S), were successfully synthesized to explore their catalytic activity in electrocatalytic H_2O_2 production. Among these, the carbon sites LZU-190(S) were predominantly activated by the introduced adjacent heteroatoms via electronic effects, resulting in much higher H_2O_2 selectivity compared to the oxazole and imine linkages. This work provides new insights into developing COFs-based electrocatalysts for efficient H_2O_2 generation.

1. Introduction

Hydrogen peroxide (H_2O_2) holds significant importance in our daily lives and modern industries with widespread applications in areas such as the pulp industry, chemical synthesis, wastewater treatment, and medical disinfection.[1-2] Currently, industrial production of H_2O_2 predominantly relies on the large-scale concentrated anthraquinone circulation process.[3-4] Another viable route involves the direct synthesis of H_2O_2 from H_2 and O_2, demonstrating high selectivity (>95%) and productivity. However, challenges such as flammability hazards and additional purification costs due to diluted carrier gas and solvent hinder large-scale H_2O_2 production through this method.[5-6] Consequently, such issues identified in these routes have motivated researchers to explore alternative, environmentally friendly, and cost-effective approaches for H_2O_2 synthesis.

Given its advantages of high-energy conversion efficiency and environmentally friendly process, electrochemical H_2O_2 production via $2e^-$ ORR is considered a burgeoning route for the facile synthesis of H_2O_2 at a low cost.[7-8] Electrocatalytic H_2O_2 synthesis offers significant advantages over traditional processes, mitigating the risk of hydrogen and oxygen mixture explosion. It requires only renewable power sources and clean water, eliminating the need for hazardous H_2 as a proton source and minimizing by-products. Despite these appealing advantages, practical processes encounter challenges from competitive reactions at cathodes, where $4e^-$ or $2e^-$ pathways could occur, resulting in the production of H_2O_2 (HO_2^-) or H_2O as products in aqueous solutions, respectively.[9-12] Therefore, there is a high demand for designing electrocatalysts to achieve high H_2O_2 production via $2e^-$ ORR.

It is generally acknowledged that the interaction between O_2 and active sites determines the pathway through which oxygen is activated.[13-14] Consequently, the final products depend highly on the adsorption energy of O_2, whether following the $4e^-$ path or the $2e^-$ path leading to H_2O_2.[15-16] Numerous explorations have confirmed that the electronic structure of catalysts is one of the most important factors influencing catalytic activity.[17-18] Therefore, various electrocatalysts with a tuneable coordination environment and controllable electronic structure have been reported to generate H_2O_2 via the $2e^-$ ORR pathway with high catalytic activity.[19-20] To date, typical electrocatalysts, including noble metals, single atoms, alloys, and carbon-based materials, have been reported as efficient catalysts for electrochemical H_2O_2 production in the literature. [21-25] However, some limitations of the above catalysts cannot be ignored and

pose barriers to their widespread use. Specifically, the scarcity of noble metals restricts their broad application in the future. Although single atom-based catalysts have drawn great attention in recent years due to atomic utilization economy, metal single sites tend to aggregate and face stability issues. Compared to noble metals and single atoms, carbon-based materials often have the characteristics of low cost, simple production, and easy regulation.[26-27] Moreover, different types of carbon-based materials with specific catalytic sites have been reported to boost the electrocatalytic performance in generating H_2O_2.[28-29] However, the main problems for them include the vague relationship between structure and property and unavoidable impurities during the synthesis process. Therefore, it is crucial to develop novel carbon materials with well-defined structures and tuneable active sites as $2e^-$ ORR electrocatalysts to understand the mechanism process and achieve the highly efficient electrochemical synthesis of H_2O_2.

Covalent organic frameworks (COFs), a class of crystalline carbon materials, are constructed using predesigned building blocks through covalent bonds.[30-31] Their ordered structures and porous skeletons make COFs versatile in various applications such as gas adsorption, organic pollutant adsorption, heterogeneous catalysis, and energy storage and conversion.[32-35] The structural predictability and precise molecular-level assembly of the active site render COFs powerful tools for controlling their chemical properties. Consequently, COFs are considered ideal candidates for electrochemical applications, leveraging their ability to integrate multiple features to enhance catalytic performance. While various COFs containing organic molecules with thiophene units, diarylamine units, or methyl groups have been reported to catalyse the $4e^-$ ORR with excellent activity, the direct electrochemical production of H_2O_2 using COFs as catalysts is still in the early stages.[36-38] Only a few examples, such as amine-linked COFs, COFs with tunable substituent groups, photo-active COFs, have been reported to achieve efficient $2e^-$ ORR.[39-42] The $2e^-$ ORR toward H_2O_2 presents more challenges than that of $4e^-$ ORR process, considering both the ability to activate oxygen and avoiding the formation of by-product water.[43-44] Therefore, achieving high selectivity for H_2O_2 in the electrochemical process relies on fabricating accurate active centres that can activate O_2 with an optimal energy barrier.

Recently, there has been increasing interest in COFs linked by C=N bonds, owing to the abundance of ligands and the potential for diverse post-treatments.[45-46] Particularly noteworthy is the formation of heterocyclic rings at the linkages of the C=N bonds, which can enhance electron transport along the frameworks and create fully conjugated structures, thereby improving overall stability.[47-49] Fortunately, our previous work revealed that a series of porous

polymers containing N-NH-, N-O-, or N-S-heterocycles can efficiently catalyse 2e$^-$-ORR.[50] Additionally, density functional theory (DFT) calculations and operando surface-enhanced infrared spectroscopy (SEIRAS) demonstrated that the activity of adjacent carbon sites can be finely controlled through atomic-scale doping with near S, N, or O atoms. Inspired by the promising catalytic properties of N-S-heterocycles units, we reported the synthesis of benzothiazole-linked COFs and benzoxazole-linked COFs to explore their catalytic activity in the electrochemical oxygen reduction process (Figure 1). The obtained LZU-190(S) exhibits

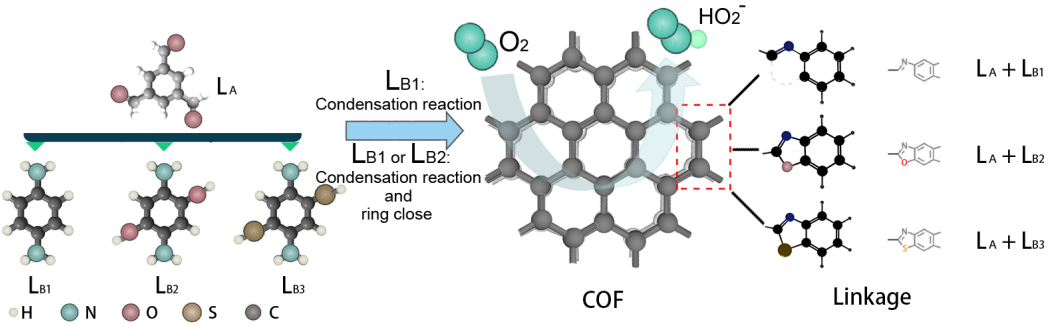

Figure 1. Scheme of the synthesis of COFs with tunable active sites for producing H_2O_2 via electrocatalytic process.

higher H_2O_2 selectivity (94.8%) compared to oxazole-linked LZU-190 (79.3%) or the corresponding undoped imine-linked LZU-1 (22.8%) in a wide potential, while maintaining satisfactory stability. Moreover, all these catalytic results outperform the performance of corresponding amorphous polymers[50], suggesting that ordered structures further facilitate electron transport and mass transfer. This work provides insights for designing more efficient COF-based catalysts in electrochemical H_2O_2 production.

2. Results and Discussion

2.1. Characterization of structures of COFs

To construct well-defined catalytic sites, three types of covalent organic frameworks (COFs) were synthesized by reacting 1,3,5-benzenetricarboxaldehyde (TFB, L_A) with organic linkers, namely, p-phenylenediamine (PPD, L_{B1}), 2,5-diamino-1,4-benzenediol dihydrochloride (DAD, L_{B2}), and 2,5-diaminobenzene-1,4-dithiol dihydrochloride (DAT, L_{B3}), respectively, as shown in Figure S4, under solvothermal conditions via a Schiff base condensation reaction (Figure 2a,

Figures S1, S2 and S3). These were denoted as LZU-1, LZU-190, and LZU-190(S). In comparison to LZU-1, LZU-190, and LZU-190(S) undergo the process of ring closure to form

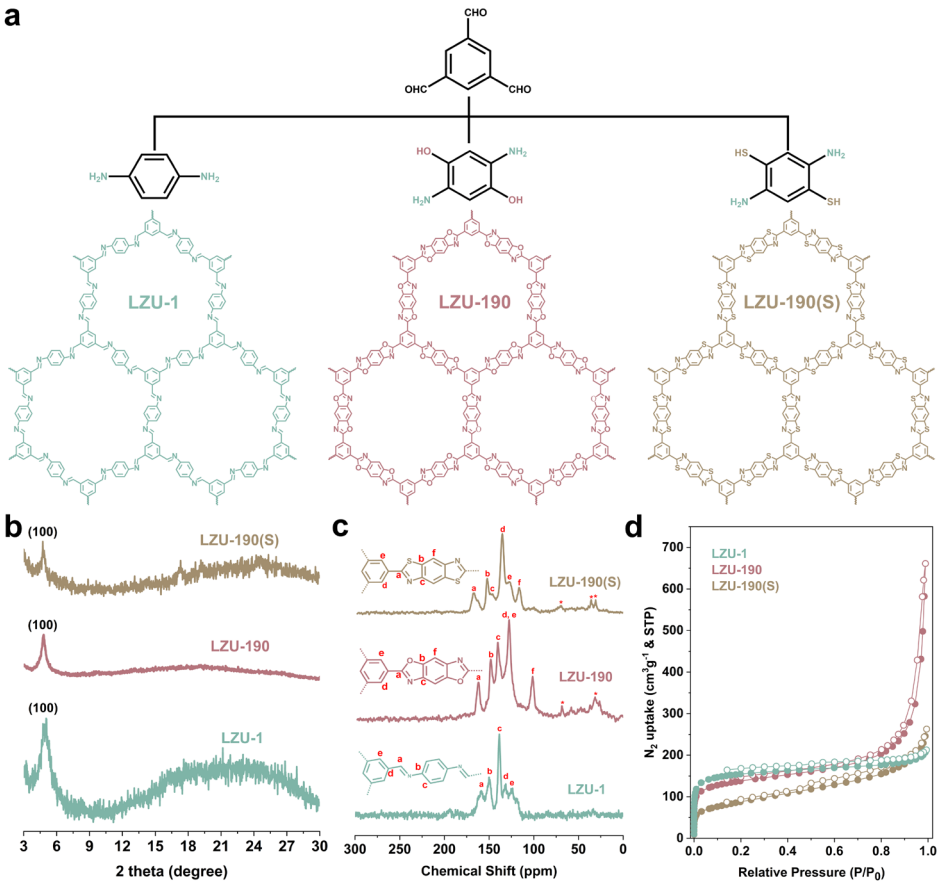

Figure 2. Schematic diagram of structures of LZU-1, LZU-190, and LZU-190(S) and corresponding structural characterization. (a) Scheme for the synthesis, and (b) PXRD patterns of LZU-1, LZU-190, and LZU-190(S). (c) ^{13}C cross-polarization magic angle spinning solid-state NMR of LZU-1, LZU-190, and LZU-190(S). Asterisks (*) indicate the peaks arising from spinning side bands. (d) N_2 adsorption isotherm (filled symbols) and desorption isotherm (open symbols) for LZU-1, LZU-190, and LZU-190(S) at 77 K.

a more stable five-membered ring heterocycle. As illustrated in Figure 2, accurate carbon active sites with a controllable coordination environment are implemented in the periodic structure of COFs, facilitating the exploration of the relationship between structures and catalytic activity. Powder X-ray diffraction (PXRD) measurements were further conducted to reveal their crystallinity. Characteristic reflection peaks were observed at 4.87°, 4.79°, and 4.77° in the

PXRD patterns of LZU-1, LZU-190, and LZU-190(S), respectively, corresponding to the (100) plane (Figure 2b).[47, 51] Considering that LZU-190(S) constructed by TFB and DAT has not been reported yet, its crystal structure was investigated in detail with the aid of Materials Studio (MS) software. Two simulated PXRD patterns representing AA and AB stacking structure were provided to confirm the structure of LZU-190(S). The experimental XRD data matched well with that of the eclipsed AA stacking model (Figure S5).

Additionally, the chemical structures of the afore mentioned COFs were initially investigated using several characterization techniques. Solid-state ^{13}C nuclear magnetic resonance (NMR) spectroscopy (Figure 2b) was employed to identify the key constituents in the COFs. As shown in Figure 2c, the signals of carbon atoms in the thiazole rings of LZU-190(S) were observed at chemical shifts of 167, 152, and 146 ppm. Other carbons in the aromatic skeletons were detectable at the chemical shift of 135, 127, and 116 ppm. Similarly, the chemical information of LZU-190 and LZU-1 can be discerned clearly, which are in according to the reported data in literatures. The signals at 162, 148, and 140 ppm can be ascribed to the carbon atoms of oxazole in LZU-190, in addition, the signals at 158, 149, 138, 131, and 124 ppm can be ascribed to the carbon atoms in LZU-1. Fourier-transform infrared (FTIR) spectroscopy is a powerful tool to confirm specific organic units in materials. Vibration signals of the thiazole rings were observed at 1667 cm^{-1} (C=N), 1308 cm^{-1} (C=C), and 1057 cm^{-1} (C-S) in LZU-190(S), while the stretching vibration of the oxazole unit was reflected at peaks of 1664 cm^{-1} (C=N), 1424 cm^{-1} (C=C), and 1121 cm^{-1} (C-O) in LZU-190 (Figures S6 and S7). In Figure S8, the notable peaks at 1622 cm^{-1} can be attributed to the signals of C=N bonds, characteristic of LZU-1. High-resolution X-ray photoelectron spectroscopy (XPS) spectra were used to detect the S or O element in LZU-190(S) and LZU-190, respectively (Figures S9, S10, and S11). To reveal the enhanced stability of COFs raised by the introduced heteroatoms, their thermal stability was investigated by thermogravimetric analysis (TGA). The results show that the LZU-190(S) catalyst exhibits

excellent thermal stability with a thermal decomposition temperature (Td, 13% weight loss) of ≈425 ° C under nitrogen (Figure S12), indicating its strong chemical robustness.

Next, the porosity of as-synthesized COFs was analyzed through isothermal N2 sorption measurements. The results revealed typical Type-I adsorption isotherms, indicating a microporous structure with a calculated pore size of 1.29 nm using the nonlocal density functional theory (NLDFT) method (Figure S13). LZU-190(O) and LZU-1 exhibited similar microporous structures with diameters of approximately 1.18 nm, 1.18 nm, respectively (Figure S13). The Brunauer–Emmett–Teller (BET) surface areas of LZU-190(S), LZU-190, and LZU-1 were measured as 305, 442, and 481 m^2 g (Figure 2d), respectively. Scanning electron microscopy (SEM) images and transmission electron microscopy (TEM) images depicted LZU-190(S), LZU-190, and LZU-1 as nanoplate-like agglomerates with diameters ranging from 200 nm to 500 nm (Figures S14 and S15). Energy-dispersive X-ray spectroscopy (EDS) mapping images were also employed to confirm the uniform distribution of constituents in LZU-1, LZU-190, and LZU-190(S) (Figure S16, S17, and S18). Specifically, C, N, and S atoms were uniformly distributed in the skeletons of LZU-190(S).

2.2. Electrochemical Performance

With the well-defined structures of the catalysts in hand, their different catalytic behaviours in oxygen activation were explored in detail. The $2e^-$-ORR performance was evaluated in a 0.5 M KOH aqueous solution using a rotating ring-disk electrode (RRDE). The H_2O_2 generated through the electrochemical reduction of oxygen on the disk electrode is quantified based on the oxidation current of hydrogen peroxide on the ring electrode potentiostated at 1.2 V (versus the reversible hydrogen electrode, the same below).[52] Figure 4a reveals ORR polarization curves of the LZU-190(S), LZU-190, and LZU-1 electrocatalysts. The disk current density (j_{disk}, solid line) represents the ORR current, while the ring current (i_{ring}, dashed line) monitors H_2O_2

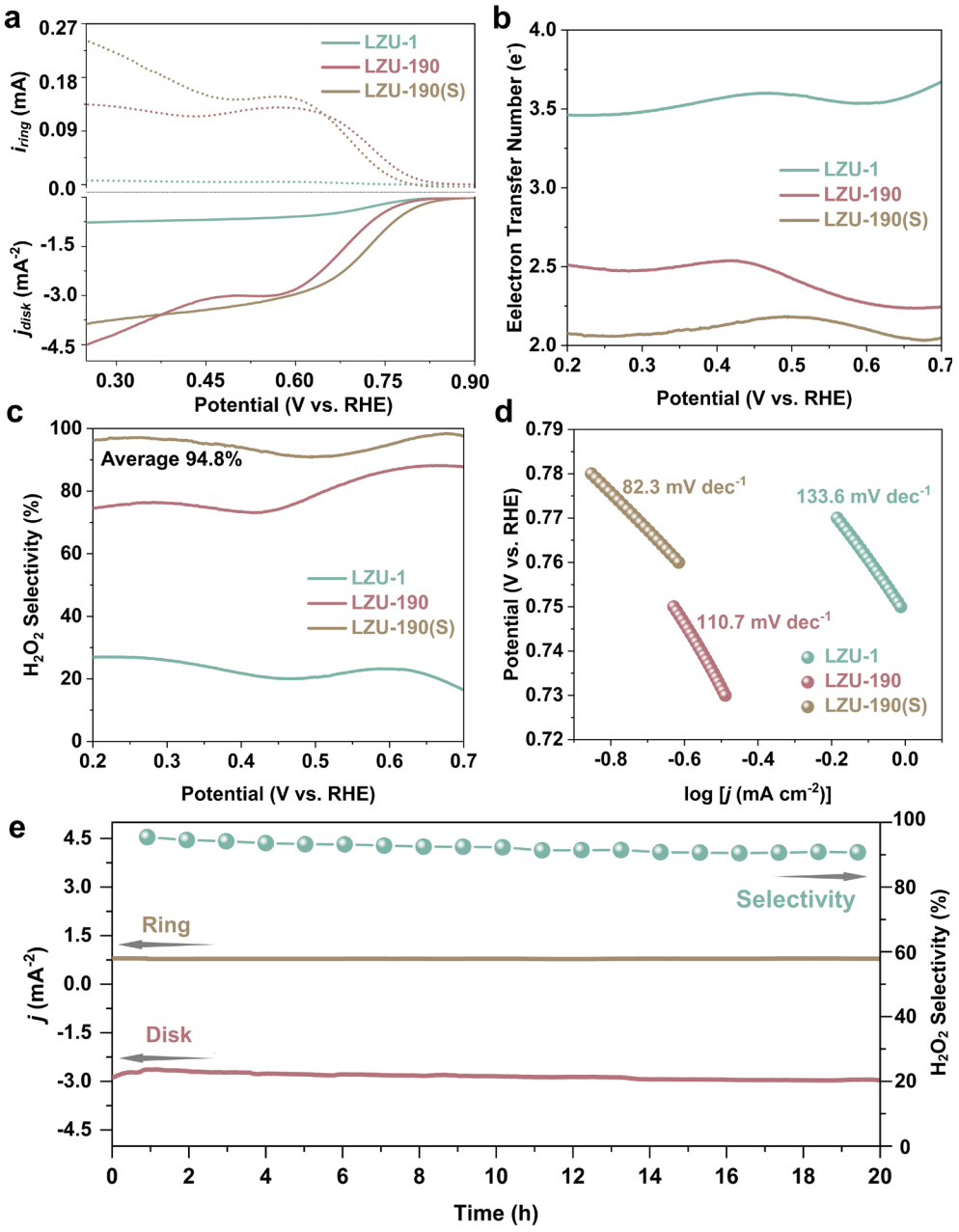

Figure 3. ORR electrocatalytic performances of LZU-1, LZU-190, and LZU-190(S) cast onto RRED in 0.5 M KOH. (a) 90% iR-compensated linear sweep voltammetry (LSV) of LZU-1, LZU-190, and LZU-190(S) recorded at 1600 rpm and a scan rate of 10 mV s^{-1}, together with the detected H_2O_2 currents on the ring electrode (upper panel) at a fixed potential of 1.2 V vs. RHE. (b) Tafel plots of LZU-1, LZU-190, and LZU-190(S). (c) Calculated H_2O_2 electron transfer number and (d) selectivity during the potential process for LZU-1, LZU-190, and LZU-

190(S). (e) Catalytic stability test of LZU-190(S) at a potential of 0.6 V vs. RHE in O_2-staurated 0.5 M KOH.

production. According to the polarization curves, the LZU-190(S) catalyst exhibits high ORR activity with an onset potential (defined as the potential at which a current density of 0.5 mA cm^{-2} is achieved) of 0.78 V, which is shifted from that of LZU-190 and LZU-1 (0.74 V and 0.66 V, respectively) and is close to the thermodynamic potential of H_2O_2 generation.[53] Increasing ring currents, decreasing disk currents, and negatively shifted onset potentials are observed in the order of LZU-1, LZU-190, and LZU-190(S), indicating a gradual tuning of the reaction pathway toward a higher fraction of $2e^-$-ORR. The specific activity Tafel plots (Figure 4b) also demonstrate that the LZU-190(S) catalyst, with the smallest slope of 82.3 mV dec^{-1}, outperforms LZU-190 (110.7 mV dec^{-1}) and LZU-1 (133.6 mV dec^{-1}), further indicating the fastest ORR kinetics of LZU-190(S) compared with the other two catalysts. To further understand the origin of catalytic activity, a plot of the calculated H_2O_2 selectivity and electron transfer number (n) as a function of applied potential is shown in Figures 4c and 4d. In a wide range of applied potentials from 0.30 to 0.70 V, LZU-190(S) exhibits the highest H_2O_2 selectivity of over 90.9%. The selectivity values of LZU-190 and LZU-1 to H_2O_2 are ~88.1% and ~22.2%, respectively, suggesting a wide range tuning of electron transfer numbers from 2.2 to 3.7, implying that the introduction of heteroatoms could effectively tune the O_2-to-H_2O_2 selectivity.[54-55]

In addition to catalytic activity, stability is another crucial consideration for a catalyst in practical applications. The electrocatalytic stability of LZU-190(S) was assessed at 0.6 V vs. RHE in 0.5 M O_2-saturated KOH under rotating conditions. Both the ring and disk electrode currents remained stable for 20 hours without significant decay (Figure 3e). The H_2O_2 selectivity, disk current, and ring current maintained 95.1, 97.1, and 98.4%, respectively. The minimal decrease in selectivity and current density suggests that the structural integrity of the

active sites remains stable during continuous electrochemical production. Moreover, these catalytic findings provide compelling evidence that the resilient crystal structure for ring-closure can effectively enhance the performance of $2e^-$-ORR and improve the durability of the framework through strong stacking interaction between layers and robust linkages.

2.3. Theoretical calculation

Density functional theory (DFT) calculations were performed to investigate the catalytic activity origins of these well-constructed COF skeletons. Three representative computational models containing thiazole, oxazole, and Schiff base units, respectively, were constructed to understand the electron environment and their effects on activating O_2 and subsequent reduction of O_2 into H_2O_2 (Figure 4). The electrostatic potential surfaces (EPSs) of LZU-190(S), LZU-190, and LZU-1 were obtained at the M06-2X/6-311G level (Figure 4a), revealing differences in their electronic structures among these COFs. LZU-190(S), characterized by its relatively more electron-rich skeleton, facilitates the adsorption of O_2 since O_2 is essentially an electron acceptor. The carbon atoms adjacent to introduced S, O, N have been identified as active sites for $2e^-$ O_2 reduction. Quantitative calculations of Hirshfeld atomic charges for the carbon sites in LZU-190(S), LZU-190, LZU-1 were performed, yielding atomic charge values of +0.0566, +0.1380, +0.0486, respectively (Figure 3b). In general, carbon sites with positive charges can serve as potential O_2 adsorption sites; however, excessive interaction between C and O can lead to overly strong adsorption of oxygens, making the subsequent reaction steps more challenging to occur. Hence, active sites with moderate adsorption ability are better candidates for catalyzing the entire ORR process to form H_2O_2. LZU-190(S), with a moderately positive charge on the identified carbon active sites (Figure d-f), is crucial for providing more favourable ORR active sites.

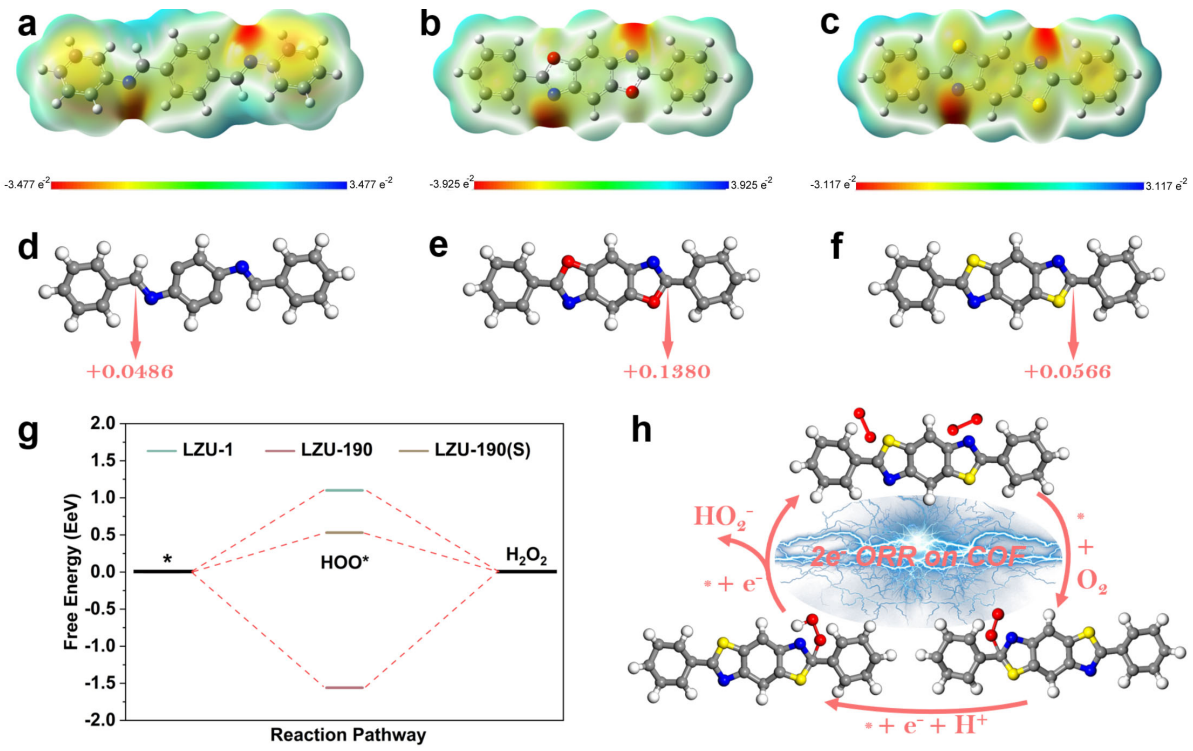

Figure 4. a-c, DFT calculations of electrostatic potential surfaces (EPSs) of LZU-190(S), LZU-190, and LZU-1 d-f, Hirshfeld atomic charges for the carbon sites in corresponding structures; g-h, DFT calculations of the of $2e^-$-ORR to H_2O_2 and schematic diagram of mechanism process. Gray, white, red, blue, and yellow spheres represent C, H, O, N, and S atoms, respectively.

Subsequently, DFT calculations about the mechanism process of $2e^-$-ORR to H_2O_2 production with respect to these three COFs were performed to further disclose their variations in ORR activity. The free energy diagram of LZU-190(S), LZU-190, and LZU-1 was constructed to illustrate the ORR process (Figure 4g). It can be observed that the O_2 → HOO* process for both LZU-190(S) and LZU-1 is endothermic and the subsequent HOO* → H_2O_2 process is exothermic. LZU-190(S) presents obvious less energy barrier compared with that of LZU-1. In contrast, LZU-190 exhibits an exothermic O_2 → HOO* process and an endothermic HOO* → H_2O_2 process, which can be attributed to the higher positive charge of active carbon sites. However, the overall energy barriers for the ORR process were determined to be 0.53 eV, 1.56 eV and 1.10 eV, respectively for LZU-190(S), LZU-190, and LZU-1. The smaller energy barrier of LZU-190(S) than that of LZU-190 indicated its higher catalytic activity. Based on the

theoretical understanding, schematic diagram of mechanism process over LZU-190(S) is presented in Figure 4h. Specifically, the carbon sites (C_{sites}) initially adsorb and activate an O_2 molecule, leading to the formation of a peroxy-adsorbed state $C_{sites}–O_2^*$. In alkaline solution, this peroxy-adsorbed state abstracts a proton from a water molecule while accepting an electron in a proton-coupled step: "$C_{sites}–OO^* + H_2O + e^- \rightleftharpoons C_{sites}\text{-}OOH^* + OH^-$". The subsequent step involves the acceptance of an electron by $C_{sites}\text{-}OOH^*$ to form $C_{sites}–OOH^{*-}$ and the cleavage of the $C_{sites}–OOH^{*-}$ bond to generate a peroxide ion HO_2^-.

3. Conclusion

In summary, three crystalline COFs containing thiazole, oxazole, and Schiff base units have been synthesized as effective electrocatalysts for $2e^-$-ORR to H_2O_2 production in alkaline electrolyte. Among them, LZU-190(S), featuring thiazole rings, demonstrates exceptional catalytic activity for $2e^-$-ORR, surpassing its counterparts LZU-190 and LZU-1. The well-defined structure of the designed COFs not only verifies the efficacy of atomic-level heteroatom doping in oxygen reduction to generate H_2O_2 but also provides a platform to elucidate their intrinsic active nature. Additionally, DFT calculations show that LZU-190(S) exhibits superior $2e^-$-ORR catalytic performance due to its moderate electron environment, which facilitates the activation of O_2 with favourable calculated energy to form H_2O_2. This study demonstrates that structure of COF can be precisely tuned and designed to achieve high-efficiency H_2O_2 production via electrocatalysis. Furthermore, numerous opportunities for synthesizing fine chemicals can be provided by using this doping strategy to enhance catalytic activity and structural stability in large-scale production.

Supporting Information

Supporting Information is available from the Wiley Online Library or from the author.

Acknowledgements

Z. Y. acknowledges the financial support from the National Natural Science Foundation of China (Grant No. 22309033), the Guizhou Provincial Science and Technology Foundation

(Grant No. [2024] ZK General 425), the Youth Scientific Research Project of Guizhou Provincial Education Department (Grant No. [2022] 125), the Academic Young Talent Foundation of Guizhou Normal University ([Grant No. 2022] B06). This research is supported by A*STAR (Nos. C233312013 and 222D800034).

Conflict of Interest

The authors declare no conflict of interest.

Data Availability Statement

The data that support the findings of this study are available from the corresponding author upon reasonable request.

References

[1] R. L. Myers, *The 100 Most Important Chemical Compounds*, Greenwood Press, London, **2007**.

[2] Y. -J. Lin, I. K. Subhajit Saha, C. -C. Wu, S. R. Barman, F. -C. Kao, Z. -H. Lin, *Nat. Commun.* **2021**, 12, 180.

[3] X. H. Xu, R. J. Sa W. Huang, Y. Sui, W. T. Chen, G. Y. Zhou, X. D. Li, Y. T. Li, H. Zhong, *ACS Catal*. **2022**, 12, 20, 12954–12963.

[4] J. M. Campos-Martin, G. J. Blanco-Brieva, L. G. Fierro, *Angew. Chem. Int. Ed*. **2006**, 45, 6962–6984.

[5] W. David, *ACS Catal.* **2018**, 8, 2, 1520-1527.

[6] H. -C. Li, Q. Wan, C. C. Du, J. F. Zhao, F. M. Li, Y. Zhang, Y. P. Zheng, M. S. Chen, K. H. L. Zhang, J. Y. Huang, G. Fu, S. Lin, X. Q. Huang, H. F. Xiong, *Nat. Commun.* **2022**, 13, 6072.

[7] Y. Y. Jiang, P. J. Ni, C. X. Chen, Y. Z. Lu, P. Yang, ; B. Kong, A. Fisher, X. Wang, *Adv. Energy Mater*. **2018**, 1801909.

[8] C. Xia, Y. Xia, P. Zhu, L. Fan, H. T. Wang, *Science* **2019**, 366, 226–231.

[9] Z. H. Xiang, Y. H. Xue, D. P. Cao, L. Huang, J. -F. Chen, L. M. Dai, *Angew. Chem. Int. Ed*. **2014**, 53, 2433–2437.

[10] D. H. Li, Y. Jia, G. J. Chang, J. Chen, H. W. Liu, J. C. Wang, Y. F. Hu, Y. Z. Xia, D. J. Yang, X. D. Yao, *Chem* **2018**, 4, 2345–2356.

[11] X. J. Long,D. H. Li, B. B. Wang, Z. J. Jiang, W. J. Xu, B. B. Wang, D. J. Yang, Y. Z. Xia, *Angew. Chem. Int. Ed*. **2019**, 131, 11491–11495.

[12] I. Kim, S. Kim, X. Jin, S. Premkumar, G. Chandra, N. -S. Lee, G. P. Mane, S. -J. Hwang, S. Umapathy, A. Vinu, *Angew. Chem. Int. Ed.* **2018**, 57, 17135–17140.

[13] P. J. Li, F. Y. Ge, Y. Yang, T. Y. Wang, X. Y. Zhang, K. Zhang, J. Y. Shen, *Angew. Chem. Int. Ed*. **2024** ,63 ,12, e202319885.

[14] Z. X. Song, X. Chi, S. Dong, B. Meng, X. J. Yu, X. L. Liu, Y. Zhou, J. Wang, *Angew. Chem. Int. Ed*. **2024**, 63, 7, e202317267.

[15] Z. P. Wang, J. H. Huang, L. Wang, Y. Y. Liu, W. H. Liu, S. L. Zhao, Z. -Q. Liu, *Angew. Chem. Int. Ed*. **2022**, 134,16, e202114696.

[16] D.S. Yu, Y. C. Ma, F. Hu, C. -C. Lin, L. L Li, H. -Y. Chen, X. P. Han, S. J. Peng, *Adv. Energy Mater.* **2021**, 11, 30, 2101242.

[17] S. Chandrasekaran, D. T. Ma, Y. Q. Ge, L. B. Deng, C. Bowen., J. Roscow, Y. Zhang, Z. Q. Lin, R. D. K. Misra, J. Q. Li, P, X. Zhang, H. Zhang, *Nano Energy* **2020**, 77, 105080.

[18] S. N. Zhao, J. -K. Li, R. Wang, J. M. Cai, S. -Q. Zang, *Adv. Mater.* **2022**, 34, 5, 2107291.

[19] G. Y. Wei, Y. X. Li, X. P. Liu, J. R. Huang, M. R. Liu, D. Y. Luan, S. Y. Gao, X. W. (David) Lou, *Angew. Chem. Int. Ed*. **2023**, 135, 47, e202313914.

[20] L. J. Li, Z. F. Hu, Y. Q. Kang, S. Y. Cao, L. P. Xu, L. Yu, L. Z. Zhang, J. C. Yu, *Nat. Commun.* **2023**, 14, 1890.

[21] E. -Y Jung, H. -J. Shin, W. H. Antink, Y. -E. Sung, T. -W H. *ACS Energy Lett.* **2020**, 5, 6, 1881–1892.

[22] D. Q. He, L. J. Zhong, S. Y. Gan, J. X. Xie, W. Wang, Z. B. Liu, W. Guo, X. Yang, L. Niu, *Electrochimi. Acta* **2021**, 371, 1, 137721.

[23] J. M. Zhang, J. Ma, T. S. Choksi, D. J. Zhou, S. B. Han, Y. -F. Liao, H. B. Yang, D. Liu, Z. P. Zeng, W. Liu, X. M. Sun, T. Y. Zhang, B. Liu, *J. Am. Chem. Soc.* **2022**, 144, 5, 2255–2263.

[24] S. -C. Lin, C. -W. Chang, M. -H. Tsai, C. -H. Chen, J. -T. Lin, C. -Y. Wu, I. -T. Kao, W. -Y. Jao, C. -H. Wang, W. -Y. Yu, C. -C. Hu, K. -H. Lin, T. -H. Yang, *Adv. Funct. Mater.* **2024**, 2314281.

[25] Y. Y. Sun, I. Sinev, W. Ju, A. Bergmann, S. Dresp, S. Kühl, C. Spöri, H. Schmies, H. Wang, D. Bernsmeier, B. Paul, R. Schmack, R. Kraehnert, B. R. Cuenya, P. Strasser, *ACS Catal*. **2018**, 8, 2844−2856.

[26] Z. Y. Lu, G. X. Chen, S. Siahrostami, Z. H. Chen, K. Liu, J. Xie, L. Liao, T. Wu, D. C. Lin, Y. Y. Liu, T. F. Jaramillo, J. K. Nørskov, Y. Cui, *Nat. Catal*. **2018**, 1, 156–162.

[27] K. -H. Wu, D. Wang, X. Y. Lu, X. F. Zhang, Z. L. Xie, Y. F. Liu, B. -J. Su, J. -M. Chen, D. -S. Su, W. Qi, S. Guo, *Chem* **2020**, 11, 1–16.

[28] T. P. Fellinger, F. Hasché, P. Strasser, M. Antonietti, *J. Am. Chem. Soc*. **2012**, 134, 4072−4075.

[29] H. W. Kim, M. B. Ross, N. Kornienko, L. Zhang, J. Gao, P. Yang, B. D. McCloskey, *Nat. Catal*. **2018**, 1, 282–290.

[30] Y. N. Shi, X. F. Zhang, H. T. Liu, J. Y. Han, Z. J. Yang, L. Gu, Z. Y. Tang, *Small*, **2020**, 16, 24, 2001998.

[31] Y. T. Zhang, Z. L. Qiao, R. Zhang, Z. Q. Wang, H. -J. Wang, J. Zhao,D. P. Cao, S. T. Wang, *Angew. Chem. Int. Ed.* **2023**, 135, e202314539

[32] X. M. Liu, G. J. H. Lim,, Y. X. Wang, L. Zhang, D. Mullangi, Y. Wu, D. Zhao, J. Ding, A. K. Cheetham, J. Wang, *Chem. Eng. J.* **2021**, 403, 126333.

[33] F. Q. Zhao, Y. Y Bai, X. Y Zhou, L. W. He, Y. N. Tao, J. C. Chen, M. X. Zhang, Q. Guo, Z. L. Ma, L. Chen, L. Zhu, T. Duan, Z. F. Chai, S. A. Wang, *Chem. Eur. J.* **2023**, 29, e2023024.

[34] T. Skorjanc, D. Shetty, A. Trabolsi, *Chem* **2021**, 7, 882–918.

[35] Q. -Y. Wang, J. Liu, M. Cao, J. -H. Hu, R. Pang, S. Wang, M. Asad, Y. -L. Wei, S. -Q. Zang, *Angew. Chem. Int. Ed.* **2022**, 133, 32, e202207130.

[36] D. H. Li, C. Y. Li, L. J. Zhang, H. Li, L. K. Zhu, D. J. Yang, Q. R. Fang, S. L. Qiu, X. D. Yao, *J. Am. Chem. Soc.* **2020**, 142, 18, 8104–8108.

[37] M. H. Liu, S. J. Liu, C. -X. Cui, Q. Y. Miao, Y. He, X. W. Li, Q. Xu, G. F. Zeng, *Angew. Chem. Int. Ed.* **2022**, 61, e20221352.

[38] Z. H. You, B. B Wang, Z. J. Zhao, Q. K. Zhang, W. C. Song, C. H. Zhang, X. J. Long Y. Z. Xia, *Adv. Mater.* **2023**, 35, 2209129.

[39] S. D. Huang, B. Y. Zhang, D. S. Wu, Y. F. Xu, H. Y. Hu, F. Duan, H. Zhu, M. L. Du, S. L. Lu, *Appl. Catal. B: Environ.* **2024**, 340, 123216.

[40] X. W. Li, Y. B. Fu, Q. Z. An, S. Yang, X. B. Yang, Q. Xu, G. F. Zeng, Z. Jiang, *Appl. Catal. B: Environ. and Energy* **2024**, 344,123611.

[41] Q. B Liao, Q. N. Sun, H. C. Xu, Y. D. Wang, Y. Xu, Z. Y. Li, J. W. Hu, D. Wang, H. J. Li, K. Xi, *Angew. Chem. Int. Ed.* **2023**, 62, e202310556.

[42] Y. Luo, B. P. Zhang, C. C. Liu, D. H. Xia, X. W. Ou, Y. P. Cai, Y. Zhou, J. Jiang, B. Han, *Angew. Chem. Int. Ed.* **2023**, 62, e202305355.

[43] S. H. An, X. W. Li, S. S. Shang, T. Xu, S. Yang, C. -X. Cui,C. J. Peng, H. L. Liu, Q. Xu, Z. Jiang,* J. Hu, *Angew. Chem. Int. Ed*. **2023**, 135, e202218742

[44] J. J. Duan, S. Chen, M. Jaroniec, S. Z. Qiao, *ACS Catal.* **2015**, 5, 5207−5234.

[45] J. L. Segura, M. J. Mancheño, F. Zamora, *Chem. Soc. Rev.*, **2016**, 45, 5635-5671.

[46] L. Cusin, H. J. Peng, A. Ciesielski, P. Samorì, *Angew. Chem. Int. Ed*. **2021**, 60, 14236–14250.

[47] P. F. Wei, M. Z. Qi, Z. P. Wang, S. Y. Ding, W. Yu, Q. Liu, L. K. Wang, H. Z. Wang, W. K. An, W. Wang, *J. Am. Chem. Soc*. **2018**, 140, 4623−4631.

[48] J. M. Seo, H. J. Noh, H. Y. Jeong, J. B. Baek, *J. Am. Chem. Soc*. **2019**, 141, 30, 11786−11790.

[49] P. J. Waller, Y. S. AlFaraj, C. S. Diercks, N. N. Jarenwattananon, O. M. Yaghi, *J. Am. Chem. Soc*. **2018**, 140, 9099−9103.

[50] Z. J. Yang, Y. Gao, L. L. Zuo, C. Long, C. Y. Yang, X. F. Zhang, *ACS Catal.* **2023**, 13, 7, 4790–4798.

[51] S. -Y. Ding, J. Gao, Q. Wang, Y. Z.†, W. -G Song, C. -Y. Su, W. Wang, *J. Am. Chem. Soc.* **2011**, 133, 49, 19816–19822.

[52] Q. R. Zhang, X. Tan, N. M. Bedford, Z. J. Han, L. Thomsen, S. Smith, R. Amal, X. Y. Lu, *Nat. Commun.* **2020**, 11, 4181.

[53] D. D. Wagman, V. B. Parker, R. H. Schumm, R. L. Nuttall, The NBS Tables of Chemical Thermodynamic Properties: Reference Data. *J. Phys. Chem. Ref. Data* **1982**, 11, 2−37−2−355.

[54] J. -M. Noel, A. Latus, C. Lagrost, E. Volanschi, P. Hapiot, *J. Am. Chem. Soc.* **2012**, 134, 2835−2841.

[55] M. -H. Shao, P. Liu, R. R. Adzic, *J. Am. Chem. Soc.* **2006**, 128, 7408−7409.

The production of hydrogen peroxide (H_2O_2) through electrocatalytic two-electron oxygen reduction reaction ($2e^-$ ORR) has been investigated using covalent organic frameworks (COFs) such as imine-linked LZU-1, oxazole-linked LZU-190, and thiazole-linked LZU-190(S). Among these, LZU-190(S) exhibits the highest selectivity for H_2O_2 compared to LZU-190(O) and LZU-1 due to the active carbon sites in LZU-190(S) being properly activated via electronic effects.

Zhongjie Yang*[1], Lulu Zuo,[3] Bifu Luo,[1] Caoyu Yang,[3] Shi-Qiang Wang [2], Litian Chew,[2] Jun Zhu,[2]* Xiaofei Zhang[2]*

Designing Heterocyclic Covalent Organic Frameworks with Tunable Electronic Structures for Efficient Electrosynthesis of Hydrogen Peroxide

ToC figure